Chemical Science

ROYAL SOCIETY OF CHEMISTRY

EDGE ARTICLE

View Article Online
View Journal | View Issue

Cite this: *Chem. Sci.*, 2024, **15**, 7603

All publication charges for this article have been paid for by the Royal Society of Chemistry

Received 9th March 2024
Accepted 15th April 2024

DOI: 10.1039/d4sc01633e

rsc.li/chemical-science

Norcorroles as antiaromatic π-electronic systems that form dimension-controlled assemblies†

Soh Ishikawa,[a] Kazuhisa Yamasumi,[a] Shinya Sugiura,[a] Shunsuke Sato,[b] Go Watanabe,[bc] Yun Hee Koo,[d] Shu Seki,[d] Yuya Bando,[a] Yohei Haketa,[a] Hiroshi Shinokubo[e] and Hiromitsu Maeda *[a]

Norcorrole derivatives with 3,4,5-trialkoxyphenyl moieties at the *meso* positions were synthesized to form various stacking assemblies in single crystals and thermotropic liquid crystals (LCs) depending on aliphatic chain lengths. Triple-decker stacking structures were formed *via* the interactions between the antiaromatic systems formed for the butoxy and dodecyloxy derivatives in the single-crystal and LC states, respectively. In particular, the LC state exhibited discotic columnar structures comprising triple deckers to exhibit high electric conductivity, as supported by molecular dynamics simulations.

Introduction

The electronic and electrooptical properties emerging from assemblies of π-electronic molecules are controlled by the arrangement of the building units.[1] π-Electronic systems form stacking structures *via* π–π interactions, which are mainly derived from dispersion forces.[2] The additional interactions that occur due to peripheral substituents, such as the van der Waals interactions among aliphatic chains, are effective in modulating the stacking structures and resulting properties for applications in molecular electronics.[3] In particular, antiaromatic systems with peripheral aliphatic chains are potentially promising candidates for electric conducting materials due to the excellent redox properties derived from the small HOMO–LUMO gaps. However, only a few antiaromatic systems have been considered as the π-electronic building units of dimension-controlled assemblies with stacking structures such as liquid crystals.[4] Moreover, their assembling behaviours were similar to those of ordinary aromatic systems because of the small antiaromaticity of the building units.

Norcorroles, porphyrin analogues whose two *meso* carbons are missing (Fig. 1 top), are promising antiaromatic π-electronic systems for forming stacking structures.[5,6] The antiaromatic property of norcorroles is derived from the 16 π-electrons in the conjugated circuit, producing attractive interactions between the antiaromatic systems through stacking, inducing stacked-ring aromaticity, for which face-to-face stacking is crucial.[6b,d,g,j] A triple-decker structure, stabilized by the stacked-ring aromaticity, was formed in the crystal structure of *meso*-phenyl-substituted Ni^{II} norcorrole, which contained outer units with concave geometries (Fig. 1 right).[6b] The assembling behaviour was modulated by the introduction of amide-substituted side chains, resulting in the formation of 1D supramolecular polymers with higher charge-carrier mobility than the aromatic counterpart.[6h] The norcorrole exhibited no obvious near infrared absorption characteristic of the face-to-face stacking in the supramolecular polymer, suggesting the deviation from face-to-face stacked arrangement. Therefore, the

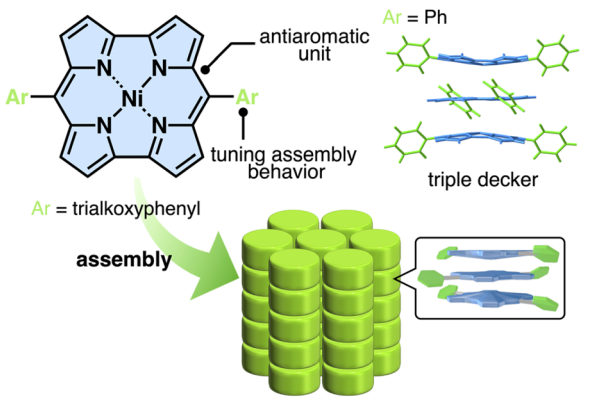

Fig. 1 Dimension-controlled assemblies of Ni^{II} norcorroles based on the interactions between antiaromatic systems.

[a]*Department of Applied Chemistry, College of Life Sciences, Ritsumeikan University, Kusatsu 525-8577, Japan. E-mail: maedahir@ph.ritsumei.ac.jp*

[b]*Department of Physics, School of Science, Kitasato University, Sagamihara 252-0373, Japan*

[c]*Department of Data Science, School of Frontier Engineering, Kitasato University, Sagamihara 252-0373, Japan*

[d]*Department of Molecular Engineering, Graduate School of Engineering, Kyoto University, Kyoto 615-8510, Japan*

[e]*Department of Molecular and Macromolecular Chemistry, Graduate School of Engineering, Nagoya University, Nagoya 464-8603, Japan*

† Electronic supplementary information (ESI) available: Synthetic procedures, analytical data, computational details and CIF files for the single-crystal X-ray structural analysis. CCDC 2288764–2288767. For ESI and crystallographic data in CIF or other electronic format see DOI: https://doi.org/10.1039/d4sc01633e

norcorrole assemblies through face-to-face stacking in dimension-controlled assemblies have not been achieved to date. The deviation from face-to-face stacked arrangement would be derived from significant hydrogen-bonding interactions between the amide units of side chains. Introduction of other side interacting moieties that have less directionality would enhance the stacking between norcorrole units. This report shows the assembly of norcorroles *via* the simple introduction of aliphatic chains, which induce van der Waals interactions, to the *meso*-aryl moieties (Fig. 1 bottom). The synergetic effects of the stacked norcorroles and introduced aliphatic chains were observed in a liquid crystal columnar assembly,[7] which exhibited nonconventional nanoscale phase-segregation as a norcorrole-based superstructure, along with enhanced electric conductivity.

Results and discussion

Synthesis and characterization

Norcorrole Ni^{II} complexes **1a–e**, bearing alkoxy units with different chain lengths at the *meso*-aryl units, were synthesized from the corresponding dipyrromethanes according to procedures found in the literature (Fig. 2 and S1†).[6b] Ni^{II}, as a diamagnetic d^8 state, was selected as a metal centre because it allowed the facile production of norcorrole frameworks. The synthesized compounds were characterized using ^1H and ^{13}C NMR and MALDI/ESI-TOF-MS. The ^1H NMR of **1a–e** in $CDCl_3$ showed antiaromatic properties as suggested by the significant upfield shifts of the β-CH signals (1.95–2.52 ppm) in contrast to those of aromatic porphyrins (9.04–9.18 ppm) (Fig. S9–13 and 17–19†). Their UV/vis absorption spectra in CH_2Cl_2 exhibited absorption bands at 427, 497 and 524 nm for **1a** and 426 and 528 nm for **1b–e**, with the alkoxy chains of four or more CH_2 units (Fig. S20†). Norcorroles **1a–e** exhibited a weak absorption band at up to ∼900 nm, which was characteristic of antiaromatic compounds.[6] TD-DFT calculation for the optimized structure of **1a** at the B3LYP/6-31G(d,p)-SDD level suggested that the absorption at 519 nm could be assigned to a CT transition band from trialkoxyphenyl units to the norcorrole core part (Fig. S42†).[8]

Upon cooling, the β-CH ^1H NMR signals of **1d** at 2.51 and 2.07 ppm at 20 °C in CD_2Cl_2 (1 mM) were shifted downfield to 3.22 and 2.80 ppm, respectively, at −30 °C, suggesting that the stacked-ring aromaticity was induced by stacking of the antiaromatic core (Fig. S77†).[6b] This result was consistent with the larger values in harmonic oscillator model of aromaticity (HOMA: 0.53, estimated based on the internal ring comprising 14 atoms) and more negative nucleus-independent chemical shift (NICS) estimated for an optimized structure of the double decker of **1a** compared to those of the monomeric **1a** (HOMA: 0.36) (Fig. S38 and 46†). The diatropic ring current indicated with clockwise arrows in the anisotropy of the induced current density (ACID) plot of the stacked **1a** dimer also supported the stacked-ring aromaticity (Fig. S48†).[8–11] The UV/vis absorption band of **1d** at ∼850 nm, which is characteristic of closely stacked norcorroles,[6b,d,g,i,j] in CH_2Cl_2 (1 mM) appeared upon cooling to −40 °C, with drastic changes at short wavelengths, suggesting the aggregation (Fig. S74†). The absorption band in the long wavelength region theoretically supported the formation of an oligomeric aggregate (Fig. S43 and 44†).[8] In contrast, **1e** rapidly formed precipitates at ∼0 °C. The cyclic voltammogram (CV) of **1b** in CH_2Cl_2 exhibited three reversible oxidation (0.16, 0.40 and 1.07 V *vs.* Ag/Ag^+) and two reversible reduction waves (−0.64 and −1.32 V) in the −2.0 to +1.3 V region (Fig. S21†). The intensities of the first two oxidation waves were approximately half of those of the other redox waves, which was similar to the previously reported results for *ortho*-unsubstituted *meso*-arylnorcorroles, suggesting the formation of a mixed-valence dimer in the first oxidation process.[6g]

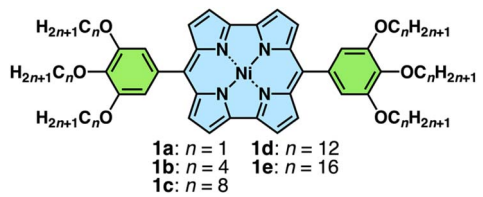

Fig. 2 Ni^{II} *meso*-(3,4,5-trialkoxyphenyl)norcorroles **1a–e**.

Solid-state assemblies

Single crystals of **1a**, **b** were prepared from C_6H_5Cl/MeOH and used for X-ray analysis.[12] In the solid state, **1a** had a square planar Ni^{II} coordination geometry with the N–Ni distances of 1.78–1.79 Å and a deviation of 0.05 Å for the mean plane (core 23 atoms), to which the *meso*-aryl rings were tilted at 45.3° (Fig. 3a(i)). In the packing diagram, stacking along the *b* axis was observed with an interplane distance of 3.67 Å and the *meso*-aryl units also showed π–π-stacking with an interplane distance of 3.56 Å. The Ni···Ni distance and angle of the **1a** plane in the columnar direction were 3.93 Å and 69.0°, respectively, with a slip distance of 1.41 Å. The long axis of the **1a** crystal corresponded to the *b* axis in the unit cell, along which the norcorroles were stacked (Fig. 3a(ii) and S29†). On the other hand, X-ray analysis of **1b** showed a triple-decker stacking structure (Fig. 3b(i)) similar to that of *meso*-phenyl-substituted norcorrole.[6b] In **1b**, the centre norcorrole was relatively planar with a deviation of 0.05 Å for the mean plane and staggered by 72.6° relative to the outer stacked molecules. The outer norcorrole units adopted a bowl-shaped conformation and a mean-plane deviation of 0.16 Å. The bowl depth defined by a Ni···mean-plane (eight β-C atoms) distance was 0.49 Å. The Ni···Ni distance and that between the two mean planes (four N atoms) of the centre and outer norcorroles were 3.00 and 3.13 Å, respectively. The close stacking of **1b** was observed with a larger overlap between the core π-planes compared to **1a**. The *meso*-aryl rings of the centre and outer **1b** were tilted at 41.9° and 48.9°/52.4°, respectively, to the mean planes (23 atoms). In the crystal of **1b**, the long axis corresponded to the *a* axis, which was the direction of the columnar assemblies of $\mathbf{1b}_3$ with a tilt (Fig. 3b(ii) and S31†). The HOMA values of **1b** (top and centre of triple decker: 0.46 and 0.53, respectively) were larger than that of **1a** (0.35), indicating that the triple decker of **1b** exhibited the stacked-ring aromaticity in contrast to slip-stacked **1a** (Fig. S32†). NICS[9,11] values in the norcorrole macrocycles of the crystal

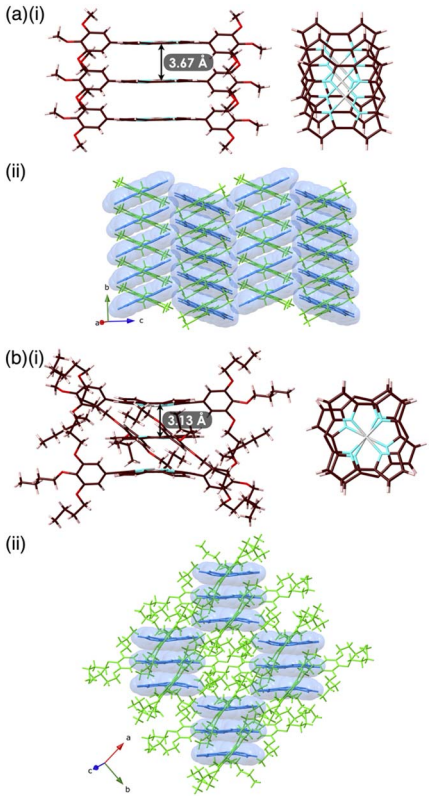

Fig. 3 (a) Single-crystal X-ray structures of (a) **1a** and (b) **1b** as (i) slip-stacked trimer and triple decker, respectively, showing the distances between two mean planes (side and core top views) and (ii) representative packing structures (blue: core unit, green: aryl unit). Atom colour codes in (i): brown, pink, cyan, red and grey refer to carbon, hydrogen, nitrogen, oxygen and nickel, respectively.

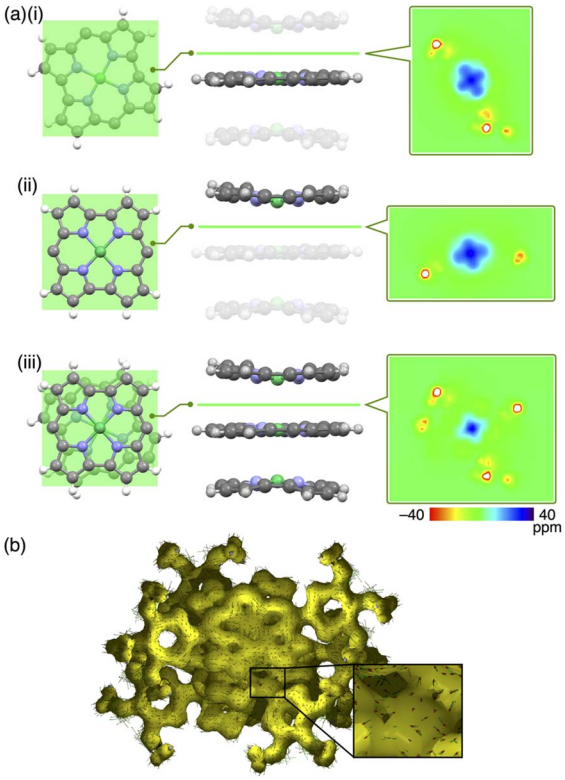

Fig. 4 (a) Arrangements of the norcorrole units in the crystal structure of **1b** as top (left) and side (centre) views and 2D NICS plots (right, ppm), estimated for the planes (left) and lines (centre), as (i) monomer (centre), (ii) monomer (top) and (iii) stacked trimer at BHLYP/6-31G(d)-SDD level and (b) ACID plot of **1b** trimer in the crystal structure. The translucent parts in the side views in (a) (i, ii) were not included in the calculations. *Meso*-aryl groups in (a) were omitted for clarity, and the butoxy groups were replaced with methoxy groups for facile calculations.

structure of **1a** (slip-stacked trimer $\mathbf{1a}_3$) at BHLYP/6-31G(d)-SDD level[8] were comparable to that of monomeric **1a**, whereas that of the crystal structure of **1b** (triple decker $\mathbf{1b}_3$, whose butyl groups were replaced with methyl groups) were significantly lower than those of monomeric **1a** (Fig. 4a, b, S46 and 47†). In addition, arrows indicating the current density in the ACID plot of $\mathbf{1a}_3$ were directed counterclockwise similar to monomeric **1a**, while those on the central norcorrole unit of $\mathbf{1b}_3$ were partially directed clockwise (Fig. 4b and S48†).[10] These results supported the contribution of stacked ring aromaticity of $\mathbf{1b}_3$.

Columnar liquid crystals based on triple deckers

Introduction of aliphatic chains to norcorrole provided mesophases (Fig. 5). Mosaic textures of polarized optical microscopy (POM) were observed for **1d** upon cooling from isotropic liquid state (Fig. 5a(i) and S51†). The mesophases formed in the dodecyloxy-substituted **1d** had transition temperatures at 10/25/45/69/79 °C (heating) and 48/20/15/–15 °C (cooling) as revealed by differential scanning calorimetry (DSC) and synchrotron X-ray diffraction (XRD), which further revealed the assembled structures in the mesophases (Fig. 6, S49, 57–59 and Table S4†). A schematic diagram of the phase transition behaviour is shown in Fig. 5b(i). In particular, the diffraction peaks were intensified upon heating, suggesting the formation of a highly ordered columnar phase (Fig. S57p–u†). The mesophase at 30 °C upon heating showed a diffraction pattern ascribable to the hexagonal columnar ($\mathrm{Col_h}$) phase with the parameters $a = 3.15$ nm, $c = 0.93$ nm and $Z = 3$ ($\rho = 0.99$) (Fig. 6a(i)), and that at 50 °C upon heating was the rectangular columnar ($\mathrm{Col_r}$) phase with the parameters $a = 5.62$ nm, $b = 3.10$ nm, $c = 0.93$ nm and $Z = 6$ ($\rho = 0.99$) (Fig. 6a(ii)), which were observed in two separated temperature ranges. The assignment of 0.93 nm as the stacking distance was confirmed by the increased intensity of the diffraction in the shearing direction, in contrast to the augmentation of other diffractions derived from the rectangular pattern in the horizontal direction (Fig. 6b). The value of 0.93 nm, which was included in both phases, could be ascribed to the repeating distance of the stacking trimeric units, as also seen in the crystal structure of **1b** (Fig. 3b). In addition, the film-state **1d** in the $\mathrm{Col_r}$ phase at the higher temperature exhibited an absorption band at ~1130 nm (Fig. S75a†), which was red-shifted compared to those of previously reported stacked dimers and aggregates (λ_{max} = 800–900 nm).[6b,d,g,i,j] The significantly red-shifted absorption for the **1d** film compared to the norcorrole double deckers was consistent with the red-shifted absorption suggested by TD-DFT calculation (Fig. S43 and

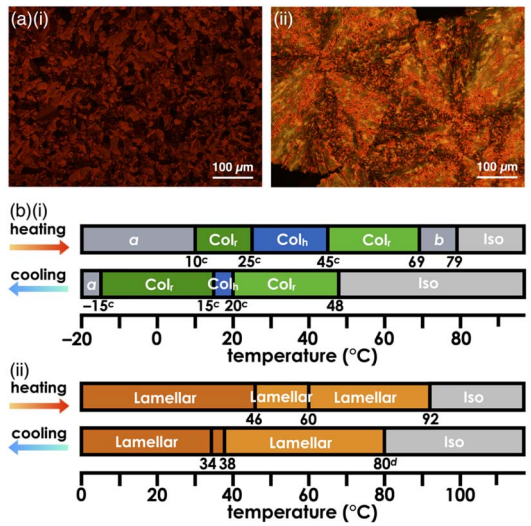

Fig. 5 (a) POM textures of (i) **1d** at 40 °C and (ii) **1e** at 80 °C upon cooling and (b) schematic diagrams of the phase transition behaviours of (i) **1d** and (ii) **1e**. Phase *a* showed no obvious peaks ascribable to the less ordered structure, whereas phase *b* exhibited a complicated diffraction pattern derived from the unidentified structure. Transition temperatures were determined by DSC without labels and also by XRD and POM labelled with *c* and *d*, respectively. Scan rates in DSC were 5 °C min^{-1} except for **1d** at 2 °C min^{-1}, which provided the transition temperatures closer to those determined by XRD.

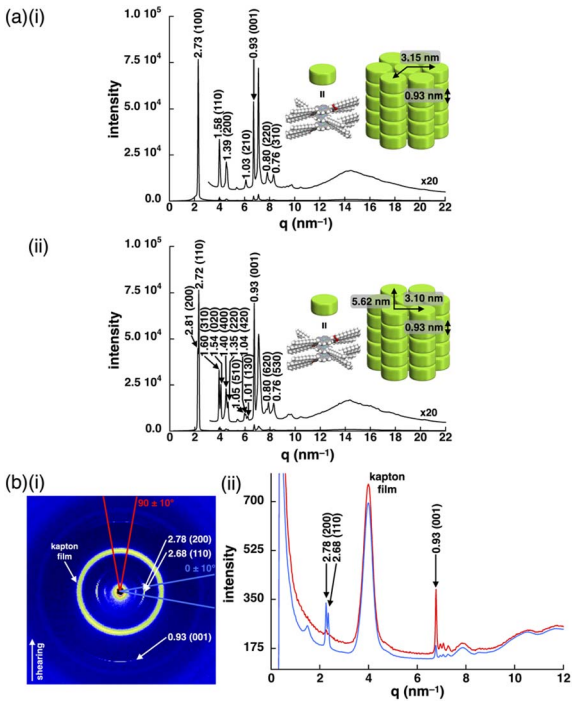

Fig. 6 (a) XRD patterns of **1d** at (i) 30 °C and (ii) 50 °C upon heating and possible assembled models and (b) XRD patterns of **1d** sheared between Kapton (polyimide) films at approximately 85 °C and cooled to r.t., including (i) 2D XRD diffraction pattern and (ii) a combined diagram showing meridional (sheared) (red) and equatorial (blue) directions. An unassigned peak close to 0.93 nm may be derived from the side aryl moieties.

44†), supporting the formation of the stacked trimer. In the higher temperature region at 69–79 °C upon heating, high fluidity was observed in the phase, which showed complicated diffractions (Fig. S57w†).

The packing structures of **1d** in the Col$_h$ and Col$_r$ phases at 30 and 50 °C, respectively, were clearly demonstrated in all-atom molecular dynamics (MD) simulations after 100 ns of the equilibration run (Fig. 7). The structures obtained by MD simulation were consistent with those determined by XRD analysis. The concave face of outer norcorrole units in **1d**$_3$ were unsuitable for stacking with another triple decker.[13] Thus, the triple deckers were not arranged in a straight line in the columnar structures (Fig. 7a right). The assembly mode was distinct from that for conventional discotic columnar structures, where π-electronic parts and aliphatic chains contribute to a 1D ordered assembly, producing more efficient intermolecular interactions and high entropy effects that exhibit fluidity, respectively. In **1d**, the proximal locations of the norcorrole units and dodecyl chains were required to convert from the Col$_h$ to Col$_r$ phase (Fig. 7a and b (left)). In this study, the concave geometries of the norcorrole triple decker resulted in nonconventional assembled structures in combination with aliphatic chains.

Effects of substituents and frameworks on assembled structures

The lengths of the aliphatic chains were essential factors in controlling the assembled structures. Hexadecyloxy-substituted **1e** exhibited the formation of mesophases with transition temperatures of 46/60/92 °C (heating) and 85/38/34 °C (cooling), as revealed by DSC and POM (Fig. 5a, b(ii), S49 and 52†). The synchrotron XRD results showed the formation of lamellar phases with repeating distances of 5.32–5.44 nm, which were

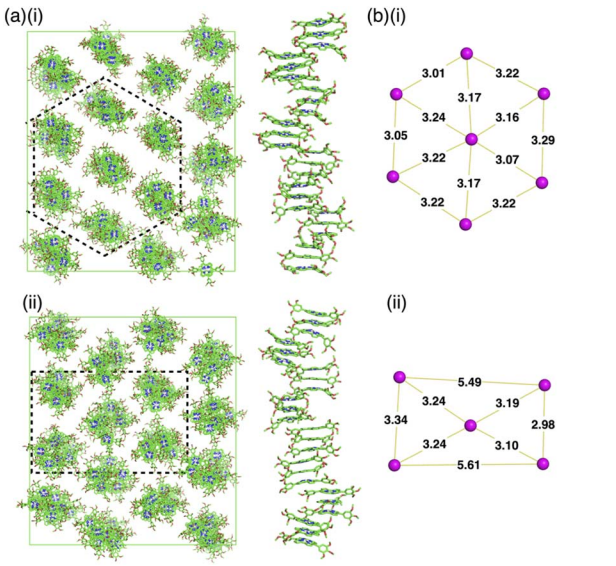

Fig. 7 (a) Snapshots of MD simulation results for **1d** and (b) arrangement of the columns with the distances (nm) (the locations are indicated with dashed lines in (a)) after 100 ns of the equilibration run (i) at 30 °C and (ii) 50 °C. The alkyl chains and hydrogens are omitted for clarity.

consistent with the molecular lengths (Fig. S60 and 61†). The diffractions at ~0.40 nm instead of that at 0.93 nm were ascribed to the stacking distances of **1e**, suggesting that **1e** did not form triple deckers in the bulk state in contrast to **1d**.[14] Compared to norcorroles **1d**, **e** with long aliphatic chains, **1c** had a higher melting point at 126 °C, at which it was decomposed upon the conversion to an isotropic liquid (Fig. S49†). The synchrotron XRD results for **1c** in the state obtained by recrystallization showed the formation of the Col_r phase, with a repeating distance of 0.93 nm (Fig. S54†), which was similar to those of **1b** and **1d** in the single-crystal and mesophase forms, respectively. In **1c** with shorter aliphatic chains, the interactions between the core π-electronic systems were predominant in forming triple deckers and their assemblies, resulting in higher crystallinity. In contrast, **1e**, with longer aliphatic chains, exhibited mesophases, wherein the stacking distance between the π units was relatively long (0.40 nm) in the lamellar phases. These longer aliphatic chains more significantly influenced on the formation of assemblies, resulting in difficulty with the close stacking of π units because of the relatively smaller interactions between the core π-electronic systems. On the other hand, **1d** with aliphatic chains of a moderate length could also form mesophases, wherein the core π-electronic system played an essential role in the aggregate formation, as Col_h and Col_r structures with close stacking.

The phase transition behaviours of analogous porphyrins **2c**–**e** with the corresponding aryl moieties to those of **1c**–**e** at the 5,15-positions, respectively, were also examined (Fig. S53b†). In contrast to **1d**, dodecyloxy **2d** formed a lamellar structure instead of columnar phases (Fig. S64†). Hexadecyloxy **2e** formed a lamellar structure, with a repeating distance similar to that of **1e**, which was maintained during the cooling and heating processes (Fig. S66†). On the other hand, octyloxy-substituted **2c**, which had a lower melting point (68 °C) than **1c**, showed no ordering behaviour during the cooling process (Fig. S62†), and a crystal-like POM texture was observed during the heating process (Fig. S50†). These observations suggested that, for the derivatives with longer aliphatic substituents, the interactions between the aliphatic groups were more significant than those between the π-planes, inducing a similar tendency to form lamellar structures. For the derivatives with moderately long aliphatic chains, distinct assembled structures were formed according to the interactions between π-planes in the norcorroles and porphyrins.

Electric conductive property

Owing to the close stacking modes in the Col_h and Col_r phases of **1d** with the wide range of continuous mesophases, the electric conductive nature of the phases was examined using flash-photolysis time-resolved microwave conductivity (FP-TRMC) measurements upon charge carrier photo-injection. The liquid crystalline sample of **1d** was investigated after heating to the isotropic liquid state and processes for phase stability at each step. The short-range proximity of the Ni^{II} norcorrole framework of crystal-state **1b** as a reference was confined to the trimer forms in the condensed phase, disrupting the 1D electric

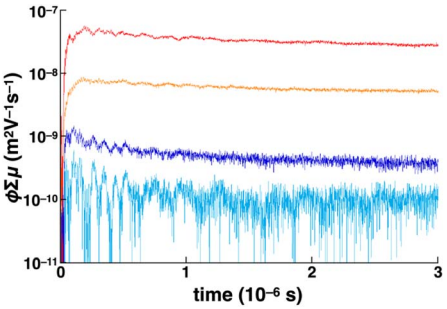

Fig. 8 Kinetic traces of transient photoconductivity observed for **1a** (light blue), **1b** (orange), **1d** (red) and **1e** (blue) upon excitation at 355 nm, 2.7×10^{15} photons cm^{-2}, at 20, 20, 25 and 50 °C, respectively.

conductive pathways. The advantages of the 1D continuous stacking modes in the mesophases of **1d** were clearly shown at 25 °C (Fig. 8). The maximum photo-conductivity of **1d** (5.2×10^{-8} m^2 V^{-1} s^{-1}) was over five times of that of **1b** and greater than those of other reported norcorrole triple deckers, including that of *meso*-phenyl derivative, in the form of single crystals.[6c,f] These observations suggested that alkoxy chains contributed to the arrangement of triple deckers, resulting into the enhanced electric conductivity. In addition, the photo-conductivities of **1d** and **1b** were significantly larger than those of slip-stacked **1e** (liquid crystal) and **1a** (crystal), respectively, probably due to the ordered arrangement of tightly stacked triple deckers. The conductivity of **1d** was also higher than the previously reported value for a norcorrole supramolecular polymer (1×10^{-8} m^2 V^{-1} s^{-1}).[6h] Upon heating **1d** from 25 °C, partial disruption of the conducting pathways was observed with an initial rapid decay until a few microseconds due to the quenching of electrons *via* residual oxygen molecules in the system (Fig. S80a†).

Conclusions

Ni^{II} norcorrole derivatives with alkoxy chains having various lengths exhibited unique assembling behaviours and enhanced electric conductivity. The norcorroles with specific alkoxy chains formed triple-decker structures, derived from the stacked-ring aromaticity, in the crystal and mesophase states. As observed in the crystal structure, concave faces of the bowl-shaped top and bottom units of the triple deckers hindered effective stacking of the norcorrole trimer. In addition, the norcorrole trimer core was surrounded by alkyl chains, resulting in a double concave discotic mesogen. In the LC state, the stacked triple-decker structure was in contact with adjacent triple deckers at the edges of both concave faces, providing a novel nanoscale phase-segregated columnar assembly *via* the interactions between the edges of the norcorrole concave faces, along with those between the core π-electronic units and side aliphatic chains. The assembling modes in the LC states were substantially different from those of ordinary aromatic systems, showing more ordered segregated structures *via* independent interactions between the core π-electronic units and aliphatic chains. Even a slight overlap between the triple deckers led to

high electric conductivity owing to the dynamic behaviours with a suitable arrangement in the LC state. Further modifications of antiaromatic π-electronic systems to obtain functional electronic materials are currently under investigation.

Data availability

Data supporting the work in this publication are available *via* the ESI† and associated crystallographic data.

Author contributions

H. M. designed and conducted the project. S. I., K. Y., S. Su., Y. H. and Y. B. carried out the synthesis, characterization and property examinations. S. Sa. and G. W. conducted the MD calculations. Y. H. K. and S. Se. evaluated electric conductivities. H. S. supported the synthesis.

Conflicts of interest

There are no conflicts of interest to declare.

Acknowledgements

This work was supported by JSPS KAKENHI Grant Numbers JP18H01968, JP22H02067 and JP23K23335 for Scientific Research (B), JP19K05444 and JP2408389 for Scientific Research (C), JP23K17951 for Challenging Research (Exploratory), JP20H05862, JP20H05863 and JP20H05867 for Transformative Research Areas (A) "Condensed Conjugation", JP19H05718 for Scientific Research on Innovative Areas "Aquatic Functional Materials", Ritsumeikan Global Innovation Research Organization (R-GIRO) project (2017–22 and 2022–27), JST SPRING Grant Number JPMJSP2101, JST CREST Grant Number JPMJCR23O1 and the Sasakawa Scientific Research Grant from the Japan Science Society. Theoretical calculations were partially performed using Research Center for Computational Science, Okazaki, Japan (21-IMS-C077, 22-IMS-C043, 22-IMS-C077, 23-IMS-C038 and 23-IMS-C069). We thank Prof. Kunihisa Sugimoto, Kindai University, and Dr Nobuhiro Yasuda, JASRI/SPring-8, for synchrotron-radiation single-crystal X-ray analysis (BL02B1 and BL40XU at SPring-8: 2021A1597 and 2021A1339), Dr Noboru Ohta (JASRI/SPring-8) for synchrotron-radiation XRD measurements (BL40B2 at SPring-8: 2016A1360, 2016B1498, 2020A1586, 2020A1664, 2021A1479, 2021B1828, 2022A1689, 2022B1546, 2023A1331 and 2023B1409), Prof. Takayuki Tanaka and Dr Akito Nakai, Kyoto University, Prof. Osamu Tsutsumi, Ritsumeikan University, for single-crystal X-ray analysis, and Prof. Hitoshi Tamiaki, Ritsumeikan University, for various measurements.

Notes and references

1 (*a*) Unimolecular and Supramolecular Electronics I: Chemistry and Physics Meet at Metal–Molecule Interfaces, *Topics in Current Chemistry*, ed. R. M. Metzger, Springer, 2012; (*b*) *Supramolecular Materials for Opto-Electronics*, ed. N. Koch, RSC, 2015.

2 C. A. Hunter and J. K. M. Sanders, *J. Am. Chem. Soc.*, 1990, **112**, 5525–5534.

3 (*a*) S. Laschat, A. Baro, N. Steinke, F. Giesselmann, C. Hägele, G. Scalia, R. Judele, E. Kapatsina, S. Sauer, A. Schreivogel and M. Tosoni, *Angew. Chem., Int. Ed.*, 2007, **46**, 4832–4887; (*b*) B. R. Kaafarani, *Chem. Mater.*, 2011, **23**, 378–396; (*c*) T. Wöhrle, I. Wurzbach, J. Kirres, A. Kostidou, N. Kapernaum, J. Litterscheidt, J. C. Haenle, P. Staffeld, A. Baro, F. Giesselmann and S. Laschat, *Chem. Rev.*, 2016, **116**, 1139–1241; (*d*) H. K. Bisoyi and Q. Li, *Chem. Rev.*, 2022, **122**, 4887–4926.

4 (*a*) S.-i. Kato, N. Takahashi, H. Tanaka, A. Kobayashi, T. Yoshihara, S. Tobita, T. Yamanobe, H. Uehara and Y. Nakamura, *Chem.–Eur. J.*, 2013, **19**, 12138–12151; (*b*) N. Takahashi, S. Kato, M. Yamaji, M. Ueno, R. Iwabuchi, Y. Shimizu, M. Nitani, Y. Ie, Y. Aso, T. Yamanobe, H. Uehara and Y. Nakamura, *J. Org. Chem.*, 2017, **82**, 8882–8896.

5 M. Bröring, S. Köhler and C. Kleeberg, *Angew. Chem., Int. Ed.*, 2008, **47**, 5658–5660.

6 (*a*) T. Ito, Y. Hayashi, S. Shimizu, J.-Y. Shin, N. Kobayashi and H. Shinokubo, *Angew. Chem., Int. Ed.*, 2012, **51**, 8542–8545; (*b*) R. Nozawa, H. Tanaka, W.-Y. Cha, Y. Hong, I. Hisaki, S. Shimizu, J.-Y. Shin, T. Kowalczyk, S. Irle, D. Kim and H. Shinokubo, *Nat. Commun.*, 2016, **7**, 13620; (*c*) T. Yoshida, D. Sakamaki, S. Seki and H. Shinokubo, *Chem. Commun.*, 2017, **53**, 1112–1115; (*d*) R. Nozawa, J. Kim, J. Oh, A. Lamping, Y. Wang, S. Shimizu, I. Hisaki, T. Kowalczyk, H. Fliegl, D. Kim and H. Shinokubo, *Nat. Commun.*, 2019, **10**, 3576; (*e*) S. Liu, H. Tanaka, R. Nozawa, N. Fukui and H. Shinokubo, *Chem.–Eur. J.*, 2019, **25**, 7618–7622; (*f*) S. Ukai, Y. H. Koo, N. Fukui, S. Seki and H. Shinokubo, *Dalton Trans.*, 2020, **49**, 14383–14387; (*g*) H. Kawashima, S. Ukai, R. Nozawa, N. Fukui, G. Fitzsimmons, T. Kowalczyk, H. Fliegl and H. Shinokubo, *J. Am. Chem. Soc.*, 2021, **143**, 10676–10685; (*h*) S. Ukai, A. Takamatsu, M. Nobuoka, Y. Tsutsui, N. Fukui, S. Ogi, S. Seki, S. Yamaguchi and H. Shinokubo, *Angew. Chem., Int. Ed.*, 2022, **61**, e202114230; (*i*) S.-Y. Liu, N. Kishida, J. Kim, N. Fukui, R. Haruki, Y. Niwa, R. Kumai, D. Kim, M. Yoshizawa and H. Shinokubo, *J. Am. Chem. Soc.*, 2023, **145**, 2135–2141; (*j*) S. Kino, S. Ukai, N. Fukui, R. Haruki, R. Kumai, Q. Wang, S. Horike, Q. M. Phung, D. Sundholm and H. Shinokubo, *J. Am. Chem. Soc.*, 2024, **146**, 9311–9317.

7 Examples for liquid crystals of porphyrinoids: (*a*) P. G. Schouten, J. F. Van Der Pol, J. W. Zwikker, W. Drenth and S. J. Picken, *Mol. Cryst. Liq. Cryst.*, 1991, **195**, 291–305; (*b*) M. Ichihara, A. Suzuki, K. Hatsusaka and K. Ohta, *Liq. Cryst.*, 2007, **34**, 555–567; (*c*) M. Stępień, B. Donnio and J. L. Sessler, *Chem.–Eur. J.*, 2007, **13**, 6853–6863; (*d*) D. Gao, J. A. Edzang, A. K. Diallo, T. Dutronc, T. S. Balaban, C. Videlot-Ackermann, E. Terazzi and G. Canard, *New J. Chem.*, 2015, **39**, 7140–7146.

8 M. J. Frisch, *et al.Gaussian 16*, Revision C.01, Gaussian, Inc., Wallingford CT, 2016.

9 P. v. R. Schleyer, C. Maerker, A. Dransfeld, H. Jiao and N. J. R. van Eikema Hommes, *J. Am. Chem. Soc.*, 1996, **118**, 6317–6318.
10 (*a*) R. Herges and D. Geuenich, *J. Phys. Chem. A*, 2001, **105**, 3214–3220; (*b*) D. Geuenich, K. Hess, F. Köhler and R. Herges, *Chem. Rev.*, 2005, **105**, 3758–3772.
11 T. Lu and F. Chen, *J. Compt. Chem.*, 2012, **33**, 580–592.
12 For the synchrotron radiation measurements: (*a*) N. Yasuda, H. Murayama, Y. Fukuyama, J. E. Kim, S. Kimura, K. Toriumi, Y. Tanaka, Y. Moritomo, Y. Kuroiwa, K. Kato, H. Tanaka and M. Takata, *J. Synchrotron Radiat.*, 2009, **16**, 352–357; (*b*) N. Yasuda, Y. Fukuyama, K. Toriumi, S. Kimura and M. Takata, *AIP Conf. Proc.*, 2010, **1234**, 147–150; (*c*) K. Sugimoto, H. Ohsumi, S. Aoyagi, E. Nishibori, C. Moriyoshi, Y. Kuroiwa, H. Sawa and M. Takata, *AIP Conf. Proc.*, 2010, **1234**, 887–890.
13 Mesophases of triple-decker complexes comprising porphyrins and phthalocyanines: (*a*) H. Miwa, N. Kobayashi, K. Ban and K. Ohta, *Bull. Chem. Soc. Jpn.*, 1999, **72**, 2719–2728; (*b*) T. Nakai, K. Ban, K. Ohta and M. Kimura, *J. Mater. Chem.*, 2002, **12**, 844–850; (*c*) Y. Zhang, W. Jiang, J. Jiang and Q. Xue, *J. Porphyrins Phthalocyanines*, 2007, **11**, 100–108; (*d*) H. Mukai, K. Hatsusaka and K. Ohta, *J. Porphyrins Phthalocyanines*, 2007, **11**, 846–856; (*e*) Y. Zhang, J. Jiang, X. Sun and Q. Xue, *Aust. J. Chem.*, 2009, **62**, 455–463.
14 In contrast to **1d**, **1e** in the film state exhibited an absorption band at 849 nm without an obvious band at ∼1130 nm, suggesting the formation of the stacked dimer which was not ordered in each layer in the lamellar phases.